Revision 1

Word count: 7653

High-pressure syntheses and crystal structure analyses of a new low-density $CaFe_2O_4$-related and $CaTi_2O_4$-type $MgAl_2O_4$ phases

Takayuki Ishii[1,2,3], Giacomo Criniti[2], Elena Bykova[2], Leonid Dubrovinsky[2], Tomoo Katsura[2,3], Hidekazu Arii[1†], Hiroshi Kojitani[1], Masaki Akaogi[1]

[1]Department of Chemistry, Gakushuin University, Mejiro, Toshima-ku, Tokyo 171-8588, Japan

[2]Bayerisches Geoinstitut, University of Bayreuth, 95440 Bayreuth, Germany

[3]Center for High Pressure Science and Technology Advanced Research, Beijing, 100094, China

[†]Present address: Faculty of Education, University of Miyazaki, 1-1 Gakuen Kibanadai Nishi, Miyazaki, 889-2192 Miyazaki, Japan

16

Abstract

Single crystals of $CaTi_2O_4$ (CT)-type, $CaFe_2O_4$ (CF)-type, and new low-density $CaFe_2O_4$(LD-CF) related $MgAl_2O_4$ were synthesized at 27 GPa and 2500 ºC, and also CT-type $MgAl_2O_4$ at 45 GPa and 1727 ºC using conventional and advanced multi-anvil technologies, respectively. The structures of CT-type and LD-CF related $MgAl_2O_4$ were analyzed by single-crystal X-ray diffraction. The lattice parameters of the CT-type phases synthesized at 27 and 45 GPa were a = 2.7903(4) Å, b = 9.2132(10) Å, and c = 9.3968(12) Å, and a = 2.7982(6) Å, b = 9.2532(15) Å, and c = 9.4461(16) Å, respectively, (Z = 4, space group: *Cmcm*) at ambient conditions. This phase has an AlO_6 octahedral site and an MgO_8 bicapped trigonal prism with two longer cation-oxygen bonds. The LD-CF related phase has a novel structure with orthorhombic symmetry (space group: *Pnma*), and lattice parameters of a = 9.207(2) Å, b = 3.0118(6) Å, c = 9.739(2) Å (Z = 4). The structural framework comprises tunnel-shaped spaces constructed by edge- and corner-sharing of AlO_6 and a 4+1 AlO_5 trigonal bipyramid, in which MgO_5 trigonal bipyramids are accommodated. The CF-type $MgAl_2O_4$ also has the same space group of *Pnma* but a slightly different atomic arrangement, with Mg and Al coordination numbers of 8 and 6, respectively. The LD-CF related phase has the lowest density of 3.50 g/cm^3 among $MgAl_2O_4$ polymorphs, despite its high-pressure synthesis from the spinel-type phase (3.58 g/cm^3), indicating that the

LD-CF related phase formed via back-transformation from a high-pressure phase during the recovery. Combined with the previously determined phase relations, the phase transition between CF- and CT-type $MgAl_2O_4$ is expected to have a steep Clapeyron slope. Therefore, CT-type phase may be stable in basaltic- and continental-crust compositions at higher temperatures than the average mantle geotherm in the wide pressure range of the lower mantle. The LD-CF related phase could be found in shocked meteorites, and used for estimating shock conditions.

Keywords

Single-crystal X-ray diffraction, crystal structure, high pressure, phase transition, spinel, post-spinel, calcium titanate, calcium ferrite

1. Introduction

$MgAl_2O_4$ spinel (Sp) is a minor but common mineral in lherzolite xenoliths from 20–50 km depths and in meteorites. The high-pressure polymorphs of $MgAl_2O_4$ with calcium ferrite (CF)- and calcium titanate (CT)-type structures are considered important and abundant components that are stable under lower-mantle conditions in Al_2O_3-rich rocks, such as basalt, upper continental crust, and sediment (e.g., Irifune et al. 1994; Ono et al. 2005; Ishii et al. 2012, 2019). High-pressure transitions in $MgAl_2O_4$ thus have been an important subject for understanding hosts of aluminum in the Earth's mantle.

High-pressure and high-temperature phase transitions in $MgAl_2O_4$ have been investigated for more than four decades (Liu 1978; Irifune et al. 1991; Funamori et al. 1998; Akaogi et al. 1999; Irifune et al. 2002; Ono et al. 2006; Enomoto et al. 2009; Kojitani et al. 2010; Kojitani et al. 2012). At temperatures of 1200 to 1600 ºC with pressures of 15 to 16 GPa, $MgAl_2O_4$ Sp decomposes to MgO periclase (Pc) + Al_2O_3 corundum (Cor) at pressures of 15 to 16 GPa. They react at pressures of 25 to 27 GPa to form CF-type $MgAl_2O_4$ (Akaogi et al. 1999; Irifune et al. 2002; Kojitani et al. 2012). At temperatures above 2000 ºC and pressures of 20 to 26 GPa, Sp first dissociates to modified ludwigite-type $Mg_2Al_2O_5$ + Cor (Kojitani et al. 2010). The dissociated phases again form a single phase with $MgAl_2O_4$ composition at pressures above

26 GPa, and this single phase has been recovered as an unknown phase at ambient conditions (Enomoto et al. 2009; Kojitani et al. 2010). Above 40 GPa, the CF phase transforms to a CT-type phase in a wide temperature range of 1200 to 3000 ºC (Funamori et al. 1998; Ono et al. 2006). The structure of CT-type $MgAl_2O_4$ has not yet been analyzed due to difficulty in collecting data suitable for analyzing the structure. It is important to analyze the structure for clarifying that the phase transformed from CF phase is CT phase. It was also reported that a poorly characterized orthorhombic phase, ε-$MgAl_2O_4$, may be possibly stable between 25 and 50 GPa at 1100–2500 ºC (Liu, 1978; Ono et al. 2006). Enomoto et al. (2009) showed that the powder X-ray diffraction pattern of the unknown $MgAl_2O_4$ phase at ambient conditions differs from those of all known $MgAl_2O_4$ phases, including ε-$MgAl_2O_4$. Thus, stabilities and structures of ε-$MgAl_2O_4$ and Enomoto et al.'s (2009) unknown phase are under debate.

In this study, we synthesized single crystals of CT-type, CF-type, and new low-density CF(LD-CF) related $MgAl_2O_4$ at 27 GPa and 2500 ºC in a single run. The pressure and temperature conditions were identical to those from which Enomoto et al. (2009) recovered the unknown phase. We also synthesized CT-type $MgAl_2O_4$ at 45 GPa and 1727 ºC using an advanced multi-anvil technique that we developed. We examined structures of the CT-type and the new LD-CF related phases of $MgAl_2O_4$ using single-crystal X-ray diffraction (XRD). We also assessed the stability of these phases in the deep mantle and shocked meteorites.

2. Experimental methods

2.1. High-pressure and high-temperature experiment at 27 GPa and 2500 ºC

Synthetic $MgAl_2O_4$ Sp (a = 8.0861(3) Å) was used as a starting material, which was synthesized from a mixture of MgO + Al_2O_3 with a molar ratio of 1:1 by heating at 1500 ºC for 24 h. The high-pressure and high-temperature synthesis was performed using a Kawai-type multi-anvil high-pressure apparatus at the Department of Chemistry, Gakushuin University, in Japan. Tungsten carbide (WC) anvils with 2.5-mm truncated edge lengths (Grade TF05, produced by Fuji Die Co., Ltd.) were used in combination with a 5 wt% Cr_2O_3-doped MgO octahedral pressure medium with a 7-mm edge length. A cylindrical Re heater was put at the center of the pressure medium. The starting material was put directly in the central part of the heater. A $LaCrO_3$ sleeve was placed outside the heater, with lids placed at both ends in the heater. Re disks were placed at the boundaries between the $LaCrO_3$ lids and sample to avoid contamination. The sample pressure was estimated based on a pressure calibration curve at 1600–1800 ºC (Ishii et al. 2011, 2012), in which the temperature effect on pressure was neglected. Temperature was measured at the central part of the outer surface of the heater using a Pt/Pt-13%Rh thermocouple up to 1800 ºC. We estimated a sample temperature of 2500 ºC by extrapolation of the power-temperature relationships up to 1800 ºC. No pressure effect on electromotive force of the thermocouple was corrected. Enomoto et al. (2009) estimated the

100 temperature error above 1800 ºC to be ±50 ºC using a Pt/Pt-13%Rh thermocouple, when the
101 power-temperature relationship below 1800 ºC was extended to higher temperatures. Pressure
102 uncertainty was estimated to be ±0.5 GPa (Ishii et al. 2011, 2012).

103 The sample was compressed to a target pressure at an almost constant rate of 1 MN/h at
104 room temperature and then heated to the target temperature of 2500 ºC at a rate of 100 ºC/min.
105 After keeping this temperature for 5 min, the sample was quenched by turning the electrical
106 power off and slowly decompressed to ambient pressure for 12 hours. Colorless and light-green
107 single crystals in the run product (see sections 2.3 and 2.4 for details) were picked up for
108 compositional and structural analyses.

109 **2.2. High-pressure and high-temperature experiment at 45 GPa and 1727 ºC**

110 The high-pressure and high-temperature experiment was conducted using the
111 Kawai-type multi-anvil apparatus with the Osugi-type guide block system, which was referred as
112 DIA-type[1] (IRIS-15) (Ishii et al. 2016, 2019) and installed at the Bayerisches Geoinstitut,
113 University of Bayreuth. TF05 WC anvils with 1°-tapering and 1.5-mm truncation were adopted

[1] This guide block system was first devised by Jiro Osugi's laboratory in the Department of Chemistry, Kyoto University. The system comprises upper and lower guide blocks, with four 45° slopes and four sliding wedges on the guide blocks. Each guide block and sliding wedge is equipped with an anvil. The six anvils in the [100] directions synchronously compress a cubic space via uniaxial force.

in combination with a Cr-doped MgO pressure medium with an edge length of 5.7 mm. The tapering technique in combination with hard WC anvils allows generation of pressures higher than 40 GPa, even using WC anvils (Ishii et al. 2016, 2017a, 2017b; Liu et al. 2017a). A Re foil heater was placed at the center of the pressure medium. A ZrO_2 thermal insulator was located outside the heater. Mo electrodes at both ends of the heater were connected with the WC anvils. A dense alumina tube (outer/inner diameter = 0.5 mm/0.3 mm; height = 2.1 mm) was inserted into the heater. A mixture of MgO-$Mg(OH)_2$-SiO_2-$Al(OH)_3$-$^{57}Fe_2O_3$ was packed in a gold tube capsule. The capsule was put inside the alumina tube, with MgO lids located at both ends. A W-3%Re/W-25%Re thermocouple measured the surface temperature of the heater.

The cell assembly was compressed to the maximum press load of 15 MN for 5 h and then heated to the target temperature of 1727 ºC. After 2 h, the assembly was quenched by turning off the electric power, and then the pressure was released for 15 hours. Temperature fluctuated within 10 ºC when the electric power was on. The generated pressure was estimated based on results of pressure calibration with separate runs, which suggested a sample pressure of 45 GPa at a press load of 15 MN and a temperature of 1727 ºC, based on alumina solubility in $MgSiO_3$ bridgmanite (Liu et al. 2017b; Ishii et al. 2016, 2017b). Pressure uncertainty based on compositional error was ±0.3 GPa. After recovering, we found a light-green crystal inside the heater, which was picked up for analyses of its composition and crystal structure.

This is the peer-reviewed, final accepted version for American Mineralogist, published by the Mineralogical Society of America.
The published version is subject to change. Cite as Authors (Year) Title. American Mineralogist, in press.
DOI: https://doi.org/10.2138/am-2021-7619. http://www.minsocam.org/

2.3. Sample characterization

Phases of the starting material of $MgAl_2O_4$ Sp were identified using a powder X-ray diffractometer (Rigaku RINT 2500V) with monochromatized Cr Kα radiation operated at 45 kV and 250 mA. Elements in crystals were checked using a field-emission-type scanning electron microscope (Zeiss LEO 1530 Gemini) with an energy dispersive X-ray spectrometer (Oxford X-Max^N) (SEM-EDS). Compositions of crystals obtained by the high-pressure and high-temperature syntheses were analyzed using an electron microprobe analyzer (EPMA) with wavelength-dispersive spectrometers (JEOL, JXA-8200). Compositional data were collected at an accelerated voltage and probe current of 15 kV and 10 nA, respectively, for 20 sec on the peaks of Mg and Al and 10 sec on the background. Natural pyrope was used as the standard material for Mg and Al. The compositions of the colorless and light-green crystals synthesized at 27 GPa and 2500 ºC were Mg:Al = 0.998(5):2.000(3) and Mg:Al = 0.995(5):2.002(2), respectively (Table 1). Origin of the light-green color may be due to chromium impurities from the $LaCrO_3$ thermal insulator or rhenium impurities from the Re heater, because crystals of this color generally were found near the heater. However, these elements were undetectable by EPMA analysis, and these impurities did not affect the single-crystal analyses.

The light-green crystal synthesized at 45 GPa has a composition of Mg:Al = 1.07(2):1.94(2) (Table 1), although the capsule with a mixture of $Mg(OH)_2$ (39.51 wt%), MgO (12.41

wt%), SiO_2 (33.31 wt%), $Al(OH)_3$ (4.80 wt%), and $^{57}Fe_2O_3$ (9.97 wt%) was put at the center of the assembly. Fe, Al-bearing bridgmanite was found in the capsule. The composition of the light green crystal thus may indicate that the crystal was formed by a reaction between the alumina tube and magnesia lids outside the capsule (see section 2.2). We were unable to determine the location of the light-green crystal due to a large deformation of the capsule. Although we confirmed that the crystal has almost no Fe based on the EPMA analysis (Table 1), the color may be due to trace amounts of Fe in the sample that were introduced when the gold capsule was broken. We also checked existence of components originated from cell materials ($LaCrO_3$, ZrO_2 and Cr_2O_3-doped MgO) by SEM-EDS, indicating no such elements in the crystal.

2.4. Single crystal X-ray structure analysis

2.4.1. Crystals synthesized at 27 GPa and 2500 ºC. A colorless single crystal with $MgAl_2O_4$ composition, approximately 50×50×50 μm^3 in size was used for the single crystal XRD measurement. The data were collected using a single-crystal X-ray diffractometer (Bruker AXS, Smart APEX2) at Gakushuin University. The diffractometer used a charge-coupled device detector in the 2θ range, up to 57.18º, with Mo Kα radiation from a rotating anode at a voltage of 50 kV and current of 240 mA. The WinGX program (Farrugia 2012) was employed for calculations of space group assignment and structure refinement. The systematic absences (*h* odd for *hk*0; *k* + *l* odd for 0*kl*; and *h*, *k*, and *l* odd for *h*00, 0*k*0, and 00*l*, respectively) were observed,

168 indicating that the space group was *Pnma* or $Pn2_1a$. The $N(Z)$ test for a center of symmetry
169 (Hargreaves and Gogoi 1966) showed the centrosymmetric space group of *Pnma*. Absorption
170 correction was empirically made using the SADABS program (Sheldrick 1996), resulting in a
171 discrepancy factor among equivalent reflections (R_{int}) of 2.65%.

172 The initial structure for the refinement was found using the direct method of the
173 SHELXL-97 program (Sheldrick 1997). Refinement of the structure was performed against $|F|^2$
174 using the full-matrix least-squares method with the scattering factors of neutral atoms
175 (International Tables for Crystallography 1992). At the initial stage of the refinement, the
176 isotropic displacement factors of all atoms were refined with the atomic positions. At the final
177 stage, the anisotropic displacement factors were refined with all independent parameters
178 simultaneously.

179 A light-green single crystal with $MgAl_2O_4$ composition, approximately $30\times30\times10$ μm^3
180 was used for single-crystal data collection. Single-crystal XRD was conducted using a 3-circle
181 Bruker diffractometer equipped with a SMART APEX CCD detector and Incoatec IμS 3.0
182 microfocus X-ray source (Ag-Kα radiation) at Bayerisches Geoinstitut, University of Bayreuth.
183 Processing of XRD data (unit cell determination and integration of reflection intensities) was
184 performed using CrysAlisPro software (Rigaku Oxford Diffraction 2019). Systematic absences

characteristic of *C*-centering ($h + k$ odd for all reflections) were observed. Empirical absorption correction was applied using spherical harmonics and implemented in the SCALE3 ABSPACK scaling algorithm, which is included in the CrysAlisPro software.

The processed XRD data showed a R_{int} value of 3.92%. The crystal structure was determined using the dual-space method in the SHELXT software. After the structure was determined, most atoms were found, and the remaining atoms were located from a series of difference Fourier map cycles. The crystal structure was refined in anisotropic approximation for all atoms against F^2 on all data using the full-matrix least squares method in the SHELXL software.

We also identified singe-crystal grains with a unit cell (a = 8.6565(13) Å, b = 2.7891(9) Å, c = 9.9509(19) Å, V = 240.25(10) Å^3) different from those belonging to the colorless and light green crystals, which were picked up from the bottom part of the heater. Analysis of systematic absences in terms of lattice-centering suggests the *Pnma* space group. Unfortunately, the data quality was not sufficient for accurate refinement of the crystal structure. Nevertheless, because the space group and values of the unit cell parameters agree with previously reported values for CF-type $MgAl_2O_4$ (Kojitani et al. 2007), we conclude that our sample contains some CF-type $MgAl_2O_4$.

This is the peer-reviewed, final accepted version for American Mineralogist, published by the Mineralogical Society of America.
The published version is subject to change. Cite as Authors (Year) Title. American Mineralogist, in press.
DOI: https://doi.org/10.2138/am-2021-7619. http://www.minsocam.org/

2.4.2. Crystal synthesized at 45 GPa and 1727°C. A light-green single crystal with $MgAl_2O_4$ composition and 40×40×20 μm^3 in size was used for single-crystal XRD data collection. The same procedure of the refinement for the light green crystal synthesized at 27 GPa and 2500 °C was adopted. The XRD data showed a R_{int} value of 2.82%. We assumed $MgAl_2O_4$ composition, although the composition was not stoichiometric and a trace amount of FeO was detected, as previously mentioned. The difference between the scattering factors of Mg and Al was very small, and the mosaicity of the crystal was high. The observed high-mosaicity caused the diffraction peak profiles to broaden at high 2θ, limiting the resolution of the structure refinement.

3. Results

Table 2 summarizes the crystallographic data of the LD-CF related and CT-type $MgAl_2O_4$ phases. Figures 1 and 2 show the structures of the LD-CF related and CT phases, respectively. Table 3 lists the average interatomic distances and coordination numbers of cations in these phases.

3.1. Crystal structure of new low-density $CaFe_2O_4$-related $MgAl_2O_4$

The XRD measurement shows that the colorless crystal has lattice parameters of a = 9.207(2) Å, b = 3.0118(6) Å, c = 9.739(2) Å, and V = 270.06(10) $Å^3$ with the space group of

Pnma. The determined structure, shown in Figure 1, has one trigonal bipyramid site for magnesium cation (MgO_5) and two crystallographically independent polyhedral sites for aluminum cations ($Al1O_6$ and 4+1 $Al2O_5$). The equivalent aluminum-oxygen polyhedra of $Al1O_{10}$ and $Al2O_8$ form double chains running parallel to the *b* axis via edge-sharing (Figure 1). The four double chains make an aluminum-oxygen polyhedral framework by corner-sharing. The magnesium cation is accommodated in the five-oxygen coordinated site in a tunnel-shaped space formed in the framework. The average Al-O distances of the $Al1O_6$ and $Al2O_5$ polyhedra are 1.952 Å and 1.860 Å, respectively, which are close to the sum of the effective ionic radii of aluminum and oxygen, 1.935 Å and 1.88 Å, calculated from $^{VI}Al^{3+}$ (0.535 Å), $^{V}Al^{3+}$ (0.48 Å), and $^{VI}O^{2-}$ (1.40 Å). The average Mg-O distance in MgO_5, 2.031 Å, is nearly the same as the sum of the effective ion radii of $^{V}Mg^{2+}$ (0.66 Å) + $^{VI}O^{2-}$, 2.06 Å. The effective coordination numbers (n_c) (Nespolo et al. 2001) of Mg and Al1, calculated using cation-five and -six neighboring oxygen bonds, are 4.72 and 5.98, respectively, indicating that those coordination environments are suitable for the cations. The n_c value of Al2 (4.23) is near four. The atomic distance of Al2-O4 (2.161 Å) is 0.3–0.4 Å longer than the other bonds, and the position of Al2 in the oxygen-trigonal bipyramid site is relatively off-centered, implying that 4 coordination is plausible for Al2 (the oxygen-tetrahedral site). The n_c value of Al2 in the oxygen tetrahedral site is 3.98, which is not significantly different from that in the oxygen-trigonal bipyramid site. This phase is

This is the peer-reviewed, final accepted version for American Mineralogist, published by the Mineralogical Society of America.
The published version is subject to change. Cite as Authors (Year) Title. American Mineralogist, in press.
DOI: https://doi.org/10.2138/am-2021-7619. http://www.minsocam.org/

237 closely related to the CF-type structure, which is based on similar atomic arrangement and
238 identical symmetry but with an extremely low density. In this paper, we therefore call this a
239 "low-density CF-related" phase, although the CT-type phase also has similar features. We
240 emphasize that, to the best of our knowledge, only a few compounds that have Mg or Al in the 5
241 coordination (trigonal bipyramid) have been found, including Al_2SiO_5 andalusite with AlO_6 and
242 AlO_5 polyhedra (Taylor 1929) and $Mg_3(PO_4)_2$ with MgO_6 and MgO_5 polyhedra (Nord and
243 Kierkegaard 1968).

244 **3.2. $CaTi_2O_4$-type structure**

245 According to the XRD results, the light green crystal synthesized at 27 GPa and 2500 ºC
246 has the orthorhombic space group *Cmcm*, with lattice parameters of a = 2.7903(4) Å, b =
247 9.2132(10) Å, c = 9.3968(12) Å and V = 241.57(5) Å^3. The $MgAl_2O_4$ phase with the space group
248 of *Cmcm* adopts the structural type of CT (Figure 2). Mg^{2+} cations surrounded by 6 oxygen
249 atoms form a distorted trigonal prism with Mg-O distances of 2.018(3) and 2.207(2) Å. Two
250 additional oxygen atoms in the distance of 2.5607(7) Å complete 8-fold bipolar prismatic
251 coordination for Mg. The prisms connect through the common triangular faces to form rods
252 parallel to the a axis. Al^{3+} cations have octahedral coordination with 6 oxygen atoms, and Al-O
253 distances vary from 1.8468(17) to 1.9858(7) Å. The octahedra connect through shared edges to

form chains parallel to the *a* axis. The MgO_8 polyhedra and AlO_6 octahedra are connected via common edges and corners.

We also obtained XRD data from the crystal synthesized at 45 GPa and 1727 ºC, showing the CT-type structure with lattice parameters of a = 2.7982(6) Å, b = 9.2532(15) Å, c = 9.4461(16) Å, and V = 244.58(8) Å^3. The volume is ~3 Å^3 larger than that of the crystal synthesized at 27 GPa and 2500 °C. This difference may be due to higher Mg content (Mg/Al=0.55) for the 45-GPa crystal than that for the 27-GPa crystal (Mg/Al=0.5), which would require Mg atoms to partially occupy the smaller octahedral Al-site. The average bond length of AlO_6 octahedra (1.936 Å) is larger than that in the 27-GPa crystal (1.928 Å), supporting incorporation of Mg into the octahedral site. Based on chemical composition analysis, this crystal may contain oxygen vacancy or hydrogen in the structure due to its apparent charge imbalance (cation: +7.96; oxygen: -8). However, we cannot draw a definite conclusion on the presence of oxygen vacancy and water in the structure due to the small grain size causing a 3.5% weight deficit in the EPMA analysis (Table 1).

4. Discussion

4.1. High-pressure crystal chemistry of $MgAl_2O_4$ polymorphs

The new LD-CF related structure is similar to CF- and CT-type structures, but it has not been described previously. Figure 3 compares the structures of $MgAl_2O_4$ polymorphs. CF- and

This is the peer-reviewed, final accepted version for American Mineralogist, published by the Mineralogical Society of America.
The published version is subject to change. Cite as Authors (Year) Title. American Mineralogist, in press.
DOI: https://doi.org/10.2138/am-2021-7619. http://www.minsocam.org/

CT-type structures consist of double chains of edge-shared AlO_6 octahedra running parallel to an orthorhombic cell axis. Both structures are classified by differences in the AlO_6-octahedral frameworks (Decker et al. 1957; Rogge et al. 1998; Yamanaka et al. 2009; Ishii et al. 2014, 2015, 2018). In the CF-type structure, an Mg cation occupies a tunnel-shaped space formed by corner-sharing of the four double chains, making 8-oxygen coordination for Mg in an oxygen-trigonal prism site with two longer Mg-oxygen bonds. The CT-type structure also makes a tunnel-shape space by corner- and edge-sharing of the four double chains, making a mirror plane parallel to the tunnel direction (Figure 2). In addition, the CT-type structure has two much longer Mg-oxygen bonds than those of the CF-type structure, making 6 coordination feasible for Mg.

In the LD-CF related structure, the coordination numbers of Al2 (4+1 coordination) and Mg (5 coordination) are lower than those in CF- and CT-type structures (6 coordination for Al and 6+2 or 8 coordination for Mg, respectively). The coordination number for Al is even smaller than the 6 coordination of the ambient pressure phase of $MgAl_2O_4$ Sp (Meducin et al. 2004). Table 4 shows molar volumes and densities of the phases with $MgAl_2O_4$ composition. The LD-CF related phase has the smallest density among these phases, even though this phase was recovered from a higher-pressure side than the stability field of $Mg_2Al_2O_5 + Al_2O_3$ (20–25 GPa and 2000–2500ºC), in which Al ions are accommodated in oxygen-octahedral sites. These facts indicate that the LD-CF related structure is of a phase which transformed from a stable phase at

high pressure and high temperature during decompression processes. This kind of back-transformation has been reported in several compounds, such as the perovskite–$LiNbO_3$ (LN)-type transitions in $FeTiO_3$, $MgSiO_3$-Al_2O_3, and $MgSiO_3$-$FeAlO_3$ systems and CF-modified CF transition in $FeCr_2O_4$ (Leinenweber et al. 1991; Akaogi et al. 2017; Ishii et al. 2014, 2017b; Liu et al. 2017b, 2019, 2020).

Our recent study reported a high-pressure phase of $MgFe_2O_4$ with a new crystal structure, which was also interpreted as a back-transformed phase. The crystal structure of the LD-CF related $MgAl_2O_4$ differs from that of this $MgFe_2O_4$ phase, which has a "Z-shape" framework consisting of edge-sharing $(Mg,Fe)O_6$ octahedra with one $(Mg,Fe)O_4$ tetrahedral and two $(Mg,Fe)O_6$ octahedral sites in the framework (Ishii et al. 2020). We emphasize that to the best of our knowledge, the LD-CF related $MgAl_2O_4$ is the first case indicating the back-transformed phase has a lower density than the ambient pressure phase. It is suggested that high-pressure crystal chemistry in AB_2O_4 is much more complicated than previously considered. The back-transformation from a high-pressure phase could be a distinct method to design novel compounds and useful for understanding high-pressure crystal chemistry.

Ishii et al. (2018) classified quenchable CF- and CT-type phases in AB_2O_4 compositions using radii of *A* and *B* cations coordinated to eight and six oxygens, respectively, showing the

CT-type phase at the *B*/*A* ionic radius ratio around 0.7. In this classification, $MgAl_2O_4$ is categorized as the CF-type (*B*/*A* ionic radius ratio = 0.6). They suggested that quenchable CT-type $MgAl_2O_4$ may be due to an Mg-Al disorder between the *A*- and *B*-sites or a different *B*/*A* ionic radius ratio at high pressures. The similar X-ray scattering factors between Mg and Al do not allow characterizing the Mg-Al disordering based on the single-crystal XRD data. However, our structural and compositional analyses of CT-type $MgAl_2O_4$ synthesized at 45 GPa and 1727 °C show the longer Al-O average bond length in the AlO_6 octahedron and the higher Mg content than those of the sample synthesized at 27 GPa and 2500 °C. These characteristics imply possible Mg-Al disordering in the CT-type structure, leading to an increase of the *B*/*A* ionic radius ratio. Compressibilities of *A*- and *B*-sites in the CT-type phase will also provide more information to understand stabilization of CT-type structure and to improve the categorization. We emphasize that $MgAl_2O_4$ is only a single compound whose high-pressure phases with both the CF- and CT-types are quenchable.

4.2. Phase stabilities of $MgAl_2O_4$ high-pressure polymorphs

Enomoto et al. (2009) reported phase relations in $MgAl_2O_4$ up to 27 GPa and 2500 °C and found an unknown phase with an $MgAl_2O_4$ composition in the run products recovered from 25.5–27 GPa and 2100–2500 °C. The pressure and temperature conditions under which we synthesized the LD-CF related phase (27 GPa and 2500 °C) fall within the region where the

unknown phase was synthesized by Enomoto et al. (2009). Furthermore, several strong diffraction peaks of the unknown phase in the powder XRD pattern observed by Enomoto et al. (2009) agree with the diffraction peaks of the present LD-CF related phase. For example, *d*-values of 4.8691 Å, 3.3442 Å, 2.6518 Å, and 2.5207 Å with relatively high intensities, as reported in Enomoto et al. (2009), correspond to diffraction peaks with indexes of 002, 202, 203, and 210, respectively, in the present LD-CF related phase. This agreement indicates that the unknown phase reported by Enomoto et al. (2009) is LD-CF related $MgAl_2O_4$. The fact that we synthesized the CF-type and CT-type phases together with the LD-CF related phase indicates that LD-CF related $MgAl_2O_4$ might be back-transformed from either of these high-pressure phases with an $MgAl_2O_4$ composition. Previous studies reported that ε-$MgAl_2O_4$, which is stable between 25 and 50 GPa (Liu 1978; Ono et al. 2006), is a candidate phase under high pressure and high temperature, but its detailed structure remains unclear. A further study with in situ X-ray observation under high pressure and high temperature is needed to reveal a high-pressure phase to produce the LD-CF related $MgAl_2O_4$ during recovery.

As shown in Table 4, our study indicates that the CT-type phase has a density of 3.864–3.912 g/cm^3 at ambient conditions, which is lower than the 3.933–3.937 g/cm^3 of the CF-type phase given by Kojitani et al. (2007) and this study. The CT-type $MgAl_2O_4$ by Ono et al. (2006) also has a smaller density of 3.927(3) g/cm^3 than that of the CF-type phase. The in situ X-ray

343 diffraction experiments at 45–117 GPa and 1200–2500ºC, however, indicated that the CT-type
344 phase is a higher-pressure phase than the CF-type phase (Ono et al. 2006). On the contrary, the
345 coordination number of Mg atoms in the CF-type phase is higher than that of the CT-type phase,
346 which suggests that the CF-type phase may be a higher-density phase, at least at ambient
347 conditions. One explanation for this contradiction is a compressibility difference between the
348 CF-type and CT-type phases. The bulk moduli of CF- and CT-type $MgAl_2O_4$, reported as 210–
349 241 GPa and 210–219 GPa, respectively (Yutani et al. 1997; Funamori et al. 1998; Irifune et al.
350 2002; Ono et al. 2006), are currently indistinguishable within the errors. Nevertheless, we
351 consider that the *c*-axis may shrink more efficiently in the CT-type structure than other
352 directions, because AlO_6 octahedra are linked by corner-sharing in the *c*-direction (AlO_6-O2-
353 AlO_6) whereas other links are made by edge-sharing, making the structure more flexible in the *c*-
354 axis (Siersch et al. 2017; Ishii et al. 2017). This possible preferred shrinkage by compression
355 would make a higher coordination number for *A*-site cation and a density crossover between the
356 two phases. Another possible explanation is the difference in thermal expansivity of CF- and CT-
357 type $MgAl_2O_4$, which has not yet been constrained experimentally. Compression experiments of
358 CF- and CT-type $MgAl_2O_4$ at high temperatures will clarify any contradictions in the density
359 difference between CF-type and CT-type phases.

This is the peer-reviewed, final accepted version for American Mineralogist, published by the Mineralogical Society of America.
The published version is subject to change. Cite as Authors (Year) Title. American Mineralogist, in press.
DOI: https://doi.org/10.2138/am-2021-7619. http://www.minsocam.org/

5. Implications

5.1. Shocked meteorites and impact craters

Shocked meteorites and impact craters bring high-pressure phases such as CF- and CT-type $FeCr_2O_4$ and LN-type $FeTiO_3$ (Dubrovinsky et al. 2009; El Goresy et al. 2010; Ishii et al. 2014; Akaogi et al. 2017) that provide important clues about pressure-temperature conditions in shock events. $MgAl_2O_4$ spinel is found in stony meteorites as a minor mineral, and therefore, it is expected that LD-CF related $MgAl_2O_4$ will be found in shocked meteorites and impact craters. It thus may serve as a possible indicator for shock conditions of 26–27 GPa and 2100–2500 °C.

5.2. Mineralogy in the deep mantle

The results, together with the present observation that the CT-type phase was located near the heater at 27 GPa and 2500 ºC, indicate that the CT-type phase is a high-temperature phase of the CF-type. The present 45-GPa synthesis of the CT phase, along with previous studies (Funamori et al. 1998; Ono et al. 2006), suggest that the CT phase is stable at pressures higher than 40 GPa. In the system $FeCr_2O_4$, the CF-CT phase transition boundary has a steep negative Clapeyron slope of about –100 MPa/K (Ishii et al. 2014). This steep slope in $FeCr_2O_4$ system originates from a small volume change between the CF and CT phases, which can cause the large dP/dT ($=\Delta S/\Delta V$) value. It is therefore likely that the CF-CT phase transition boundary in

the $MgAl_2O_4$ system also has a steep *dP/dT* slope due to the small volume difference between the CF and CT phases (Table 4).

Ono et al. (2005) synthesized the CT phase in a basaltic crust composition at 143 GPa, which is higher than the core-mantle boundary pressure, suggesting that the CT phase is stable around the bottom of the core-mantle boundary. If the steep negative boundary is common to CF–CT transitions, the CT phase may be stable at high temperatures, such as those found in upwelling plumes with basaltic and continental-crust compositions in the lower mantle (Ricolleau et al. 2010; Ishii et al. 2012, 2019). Thus, it is valuable for better understanding of the mantle structure and dynamics to investigate the stability of CT phases with more realistic compositions in the lower mantle across a wide temperature range.

Acknowledgements

We thank K. Mochida and A. Aimi for their help with the single-crystal structure analysis. We also thank Alan B. Woodland, an anonymous referee, and a technical editor for valuable comments and suggestions and the Associate Editor R. Sinmyo for editorial handling. M. Akaogi was supported by Grants-in-Aid (nos. 22340163, 25287145, and 17H02986) from the Japan Society for the Promotion of Science and from the Strategic Research Foundation at Private Universities program supported by the Ministry of Education, Culture, Sports, and

394 Technology of Japan. T. Ishii was supported by the Research Fellowship for Young Scientists
395 from the Japan Society for the Promotion of Science, the Alexander von Humboldt Postdoctoral
396 Fellowship, and the German Research Foundation (no. IS350/1-1). This project was also
397 supported by the funding from the European Research Council (ERC) under the European
398 Union's Horizon 2020 research and innovation programme (UltraLVP, Proposal No. 787 527).

399

400 **References cited**

401 Akaogi, M., Hamada, Y., Suzuki, T., Kobayashi, M., and Okada, M. (1999). High pressure
402 transitions in the system $MgAl_2O_4$–$CaAl_2O_4$: a new hexagonal aluminous phase with
403 implication for the lower mantle. Physics of the Earth and Planetary Interiors, 115(1), 67-77.

404 Akaogi, M., Abe, K., Yusa, H., Ishii, T., Tajima, T., Kojitani, H., Mori, D., and Inaguma, Y.
405 (2017). High-pressure high-temperature phase relations in $FeTiO_3$ up to 35 GPa and 1600 C.
406 Physics and Chemistry of Minerals, 44(1), 63-73.

407 Chen, M., Shu, J., Mao, H. K., Xie, X., & Hemley, R. J. (2003). Natural occurrence and
408 synthesis of two new postspinel polymorphs of chromite. Proceedings of the National
409 Academy of Sciences, 100, 14651-14654.

410 Decker, B.F., and Kasper, J.S. (1957) The structure of calcium ferrite. Acta Crystallographica,
411 10, 332-337.

412 Dubrovinsky, L. S., El Goresy, A., Gillet, P., Wu, X., & Simionivici, A. (2009). A novel natural
413 shock-induced high-pressure polymorph of $FeTiO_3$ with the Li-niobate structure from the Ries
414 Crater, Germany. Meteoritics & Planetary Science , *72*, 5094.

El Goresy, A., Dubrovinsky, L., Gillet, P., Graup, G., & Chen, M. (2010). Akaogiite: An ultra-dense polymorph of TiO_2 with the baddeleyite-type structure, in shocked garnet gneiss from the Ries Crater, Germany. American Mineralogist, 95, 892-895.

Enomoto, A., Kojitani, H., Akaogi, M., and Yusa, H. (2009) High-pressure transitions in $MgAl_2O_4$ and a new high-pressure phase of $Mg_2Al_2O_5$. Journal of Solid State Chemistry, 182, 389-395, doi:10.1016/j.jssc.2008.11.015.

Farrugia, L.J. (2012) WinGX and ORTEP for Windows: an update. Journal of Applied Crystallography, 45, 849-854.

Funamori, N., Jeanloz, R., Nguyen, J. H., Kavner, A., Caldwell, W. A., Fujino, K., Miyajima, N. Shinmei, T., and Tomioka, N. (1998). High pressure transformations in $MgAl_2O_4$. Journal of Geophysical Research: Solid Earth, 103(B9), 20813-20818.

Hargreaves, A. T., and Gogoi, B. N. (1966). A modified N (z) test for crystal symmetry. Acta Crystallographica, 21(1), 26-28.

Irifune, T., Fujino, K., and Ohtani, E. (1991). A new high-pressure form of $MgAl_2O_4$. Nature, 349(6308), 409.

Irifune, T., and Ringwood, A. E. (1993). Phase transformations in subducted oceanic crust and buoyancy relationships at depths of 600–800 km in the mantle. Earth and Planetary Science Letters, 117(1-2), 101-110.

Irifune, T., Ringwood, A. E., and Hibberson, W. O. (1994). Subduction of continental crust and terrigenous and pelagic sediments: an experimental study. Earth and Planetary Science Letters, 126(4), 351-368.

Irifune, T., Naka, H., Sanehira, T., Inoue, T., and Funakoshi, K. (2002). In situ X-ray observations of phase transitions in $MgAl_2O_4$ spinel to 40 GPa using multianvil apparatus with sintered diamond anvils. Physics and Chemistry of Minerals, 29(10), 645-654.

Ishii, T., Kojitani, H., and Akaogi, M. (2011). Post-spinel transitions in pyrolite and Mg_2SiO_4 and akimotoite–perovskite transition in $MgSiO_3$: precise comparison by high-pressure high-temperature experiments with multi-sample cell technique. Earth and Planetary Science Letters, 309(3-4), 185-197.

Ishii, T., Kojitani, H., and Akaogi, M. (2012). High-pressure phase transitions and subduction behavior of continental crust at pressure–temperature conditions up to the upper part of the lower mantle. Earth and Planetary Science Letters, 357, 31-41.

Ishii, T., Kojitani, H., Tsukamoto, S., Fujino, K., Mori, D., Inaguma, Y., Tsujino, N., Yoshino, T., Yamazaki, D., Higo, Y., Funakoshi, K., and Akaogi, M. (2014) High-pressure phase transitions in $FeCr_2O_4$ and structure analysis of new post-spinel $FeCr_2O_4$ and $Fe_2Cr_2O_5$ phases with meteoritical and petrological implications. American Mineralogist, 99, 1788-1797. DOI: 10.2138/am.2014.4736.

Ishii, T., Kojitani, H., Fujino, K., Yusa, H., Mori, D., Inaguma, Y., Matsushita, Y., Yamaura, K., and Akaogi, M. (2015) High-pressure high-temperature transitions in $MgCr_2O_4$ and crystal structures of new $Mg_2Cr_2O_5$ and post-spinel $MgCr_2O_4$ phases with implications for ultra-high pressure chromitites in ophiolites, American Mineralogist, 100, 59-65. DOI: 10.2138/am.2014.4736.

Ishii, T., Shi, L., Huang, R., Tsujino, N., Druzhbin, D., Myhill, R., Li, Y., Lin, W., Yamamoto, T., Miyajima, N., Kawazoe, T., Nishiyama, N., Higo, Y., Tange, Y., and Katsura, T. (2016). Generation of pressures over 40 GPa using Kawai-type multi-anvil press with tungsten carbide anvils. Review of Scientific Instruments, 87(2), 024501.

Ishii, T., Yamazaki, D., Tsujino, N., Xu, F., Liu, Z., Kawazoe, T., Yamamoto, T., Druzhbin, D., Wang, L., Higo, Y., Tange, Y., Yoshino, T., and Katsura, T. (2017). Pressure generation to 65

462 GPa in a Kawai-type multi-anvil apparatus with tungsten carbide anvils. High Pressure
463 Research, 37(4), 507-515.

464 Ishii, T., Tsujino, N., Arii, H., Fujino, K., Miyajima, N., Kojitani, H., Kunimoto, T., and Akaogi,
465 M. (2017). A shallow origin of so-called ultrahigh-pressure chromitites, based on single-
466 crystal X-ray structure analysis of the high-pressure $Mg_2Cr_2O_5$ phase, with modified
467 ludwigite-type structure. American Mineralogist: Journal of Earth and Planetary Materials,
468 102(10), 2113-2118.

469 Ishii, T., Sinmyo, R., Komabayashi, T., Ballaran, T. B., Kawazoe, T., Miyajima, N., Hirose, K.,
470 and Katsura, T. (2017). Synthesis and crystal structure of $LiNbO_3$-type $Mg_3Al_2Si_3O_{12}$: A
471 possible indicator of shock conditions of meteorites. American Mineralogist: Journal of Earth
472 and Planetary Materials, 102(9), 1947-1952.

473 Ishii, T., Sakai, T., Kojitani, H., Mori, D., Inaguma, Y., Matsushita, Y., Yamaura, K., and
474 Akaogi, M. (2018). High-Pressure Phase Relations and Crystal Structures of Postspinel Phases
475 in MgV_2O_4, FeV_2O_4, and $MnCr_2O_4$: Crystal Chemistry of AB_2O_4 Postspinel Compounds.
476 Inorganic chemistry, 57, 6648-6657.

477 Ishii, T., Kojitani, H., and Akaogi, M. (2019). Phase relations of harzburgite and MORB up to
478 the uppermost lower mantle conditions: Precise comparison with pyrolite by multi-sample cell

high pressure experiments with implication to dynamics of subducted slabs. Journal of Geophysical Research: Solid Earth, 124(4), 3491-3507.

Ishii, T., Liu, Z., and Katsura, T. (2019). A Breakthrough in Pressure Generation by a Kawai-Type Multi-Anvil Apparatus with Tungsten Carbide Anvils. Engineering, 5(3), 434-440.

Ishii, T., Miyajima, N., Sinmyo, R., Kojitani, H., Mori, D., Inaguma, Y., and Akaogi, M. (2020). Discovery of New Structured Post-Spinel $MgFe_2O_4$: Crystal Structure and High-Pressure Phase Relations. Geophysical Research Letters, 47(6), e2020GL087490.

Kojitani, H., Hisatomi, R., and Akaogi, M. (2007). High-pressure phase relations and crystal chemistry of calcium ferrite-type solid solutions in the system $MgAl_2O_4$-Mg_2SiO_4. American Mineralogist, 92(7), 1112-1118.

Kojitani, H., Enomoto, A., Tsukamoto, S., Akaogi, M., Miura, H., and Yusa, H. (2010). High-pressure high-temperature phase relations in $MgAl_2O_4$. In Journal of Physics: Conference Series (Vol. 215, No. 1, p. 012098). IOP Publishing.

Kojitani, H., Ishii, T., and Akaogi, M. (2012). Thermodynamic investigation on phase equilibrium boundary between calcium ferrite-type $MgAl_2O_4$ and MgO+ α-Al_2O_3. Physics of the Earth and Planetary Interiors, 212, 100-105.

Leinenweber, K., Utsumi, W., Tsuchida, Y., Yagi, T., and Kurita, K. (1991). Unquenchable high-pressure perovskite polymorphs of $MnSnO_3$ and $FeTiO_3$. Physics and Chemistry of Minerals, 18(4), 244-250.

Liu, L. G. (1978). A new high-pressure phase of spinel. Earth and Planetary Science Letters, 41(4), 398-404.

Liu Z., Ishii T., and Katsura T. (2017). Rapid decrease of $MgAlO_{2.5}$ component in bridgmanite with pressure. Geochemical Perspective Letters, 5, 12-18.

Liu, Z., Nishi, M., Ishii, T., Fei, H., Miyajima, N., Ballaran, T. B., Ohfuji, H., Sakai, T., Wang, L., Shcheka, S., Arimoto, T., Tange, Y., Higo, Y., Irifune, T., and Katsura, T. (2017). Phase relations in the system $MgSiO_3$-Al_2O_3 up to 2300 K at lower mantle pressures. Journal of Geophysical Research: Solid Earth, 122(10), 7775-7788.

Liu, Z., Dubrovinsky, L., McCammon, C., Ovsyannikov, S. V., Koemets, I., Chen, L., Cui, Q., Su, N., Cheng, J., Cui, T., Liu, B., and Katsura, T. (2019). A new $(Mg_{0.5}Fe_{0.5}^{3+})(Si_{0.5}Al_{0.5}^{3+})O_3$ $LiNbO_3$-type phase synthesized at lower mantle conditions. American Mineralogist, 104(8), 1213-1216.

510 Liu, Z., McCammon, C., Wang, B., Dubrovinsky, L., Ishii, T., Bondar, D., Nakajima, A., Tange,
511 Y., Higo, Y., Cui, T., Liu, B., and Katsura, T. (2020) Stability and solubility of the $FeAlO_3$
512 component in bridgmanite at uppermost lower mantle conditions. Journal of Geophysical
513 Research: Solid Earth, 125(2). https://doi.org/10.1029/2019JB018447

514 Meducin, F., Redfern, S. A., Le Godec, Y., Stone, H. J., Tucker, M. G., Dove, M. T., and
515 Marshall, W. G. (2004). Study of cation order-disorder in $MgAl_2O_4$ spinel by in situ neutron
516 diffraction up to 1600 K and 3.2 GPa. American Mineralogist, 89(7), 981-986.

517 Nespolo, M., Ferraris, G., and Hoppe, R. (2001) Charge distribution analysis of ceramic
518 materials. Journal of Ceramic Processing Research, 2, 38-44.

519 Nord, A. G., and Kierkegaard, P. E. D. E. R. (1968). The crystal structure of $Mg_3(PO_4)_2$. Acta
520 Chemica Scandinavica, 22, 1466-1474.

521 Ono, S., Ohishi, Y., Isshiki, M., and Watanuki, T. (2005). In situ X-ray observations of phase
522 assemblages in peridotite and basalt compositions at lower mantle conditions: Implications for
523 density of subducted oceanic plate. Journal of Geophysical Research: Solid Earth, 110(B2).

524 Ono, S., Kikegawa, T., and Ohishi, Y. (2006). The stability and compressibility of $MgAl_2O_4$
525 high-pressure polymorphs. Physics and chemistry of minerals, 33(3), 200-206.

526 Osugi, J., Shimizu, K., Inoue, K., and Yasunami, K. (2006) A compact cubic anvil high pressure
527 apparatus. The Review of Physical Chemistry Japan, 34(1):1-6.

528 Ricolleau, A., Perrillat, J. P., Fiquet, G., Daniel, I., Matas, J., Addad, A., Menguy, N., Cardon,
529 H., Mezouar, M., and Guignot, N. (2010). Phase relations and equation of state of a natural
530 MORB: Implications for the density profile of subducted oceanic crust in the Earth's lower
531 mantle. *Journal of Geophysical Research: Solid Earth*, *115*(B8).

532 Rigaku Oxford Diffraction (2019) CrysAlisPro Software system, version 1.171.40.57a, Oxford,
533 UK.

534 Rogge, M.P., Caldwell, J.H., Ingram, D.R., Green, C.E., Geselbracht, M.J., and Siegrist, T.
535 (1998) A new synthetic route to pseudo-brookite-type $CaTi_2O_4$. Journal of Solid State
536 Chemistry, 141, 338–342.

537 Shannon, R.D. (1976) Revised effective ionic radii and systematic studies of interatomic
538 distances in halides and chalcogenides. Acta Crystallographica, A32, 751-767.

539 Sheldrick, G.M. (1996) SADABS. Program for empirical absorption correction of area detector
540 data. Institut für Anorganische Chemie, University of Göttingen, Germany.

541 Sheldrick, G.M. (1997) SHELX-97 (computer program), University of Göttingen, Germany.

542 Siersch, N.C., Ballaran, T.B., Uenver-Thiele, L., and Woodland, A.B. (2017). Compressibility
543 and high-pressure structural behavior of $Mg_2Fe_2O_5$. American Mineralogist, 102, 845-850.

544 Taylor, W. H. (1929). XIII. The Structure of Andalusite, Al_2SiO_5. Zeitschrift für
545 Kristallographie-Crystalline Materials, 71(1-6), 205-218.

546 Toebbens, D.M., Stuesser, N., Knorr, K., Mayer, H.M., and Lampert, G. (2001) Calculated from
547 ICSD using POWD-12++, Mater. Sci. Forum, 378, 288.

548 Tsirelson, V. G., Avilov, A. S., Abramov, Y. A., Belokoneva, E. L., Kitaneh, R., and Feil, D.
549 (1998). X ray and Electron Diffraction Study of MgO. Acta Crystallographica Section B,
550 54(1), 8-17.

551 Wilson, A.J.C., Eds. (1992) International Tables for Crystallography, vol. C, Dodrecht: Kluwer
552 Academic Publishers.

553 Yamanaka, T., Uchida, A., and Nakamoto, Y. (2009) Structural transition of post-spinel phases
554 $CaMn_2O_4$, $CaFe_2O_4$ and $CaTi_2O_4$ under high-pressures up to 80 GPa. American Mineralogist,
555 93, 1874-1881.

556 Yutani, M., Yagi, T., Yusa, H., and Irifune, T. (1997). Compressibility of calcium ferrite-type
557 $MgAl_2O_4$. Physics and Chemistry of Minerals, 24(5), 340-344.

558 **Figure captions**

559

560 **Figure 1.** The refined structure of low-density $CaFe_2O_4$-related $MgAl_2O_4$, revealed by single-crystal X-
561 ray diffraction analysis. (a) Crystal structure viewed along the *b* axis. A solid rectangular box shows the
562 unit cell. (b) Detailed coordination environments of Mg and Si sites. Red spheres are oxygen atoms.

563

564 **Figure 2.** The refined structure of $CaTi_2O_4$-type $MgAl_2O_4$ synthesized at 27 GPa and 2500 °C, revealed
565 by single-crystal X-ray diffraction analysis. (a) Crystal structure viewed along the *a* axis. A solid
566 rectangular box shows the unit cell. (b) Detailed coordination environments of Mg and Si sites. Red
567 spheres are oxygen atoms.

568

569 **Figure 3.** Structural comparison among $MgAl_2O_4$ compounds at ambient conditions. Density of
570 $MgAl_2O_4$ phase increases from left to right. The numbers below the structures are coordination numbers
571 for Mg and Al. Dashed lines are the longest oxygen-cation bonds in the polyhedra, which contribute less
572 to the coordination of the cations. Blue octahedra and yellow trigonal bipyramids accommodate Al
573 cations. Orange spheres are Mg cations. In the Sp (spinel) structure, Mg cations are accommodated in

574 tetrahedral sites. Red spheres are oxygen atoms. Solid lines are unit cells. CF: calcium ferrite, CT:

575 calcium titanate, LD-CF: low-density calcium ferrite-related.

Table 1. Chemical compositions of new low-density $CaFe_2O_4$-related and $CaTi_2O_4$-type $MgAl_2O_4$.

Phase	MgO	Al_2O_3	FeO	SiO_2	Total	Mg	Al	Fe	Si
LD-CF-related	26.97(20)	71.75(60)	-	-	98.72(74)	0.998(5)	2.001(3)	-	-
CT-type (27 GPa and 2500 °C)	26.90(31)	71.92(88)	-	-	98.82(117)	0.995(5)	2.002(2)	-	-
CT-type (45 GPa and 1727 °C)	29.17(25)	66.81(122)	0.27(10)	0.30(7)	96.55(104)	1.069(19)	1.939(15)	0.005(2)	0.007(2)

576 Number in parentheses represents standard deviation for the last digit (s). Abbreviations: LD-CF, low-
577 density $CaFe_2O_4$; CT, $CaTi_2O_4$. Synthesized conditions for CT phases are shown in parentheses.

578 **Table 2.** Crystallographic data of new low-density $CaFe_2O_4$-related and $CaTi_2O_4$-type $MgAl_2O_4$.

Crystal structure	Low-density $CaFe_2O_4$-related	[a]$CaTi_2O_4$-type	[b]$CaTi_2O_4$-type
Crystal color	Colorless	Light green	Light green
Crystal system	Orthorhombic	Orthorhombic	Orthorhombic
Lattice parameter	a = 9.207(2) Å	a = 2.7903(4) Å	a = 2.7982(6) Å
	b = 3.0118(6) Å	b = 9.2132(10) Å	b = 9.2532(15) Å
	c = 9.739(2) Å	c = 9.3968(12) Å	c = 9.4461(16) Å
	V = 270.06(10) Å^3	V = 241.57(5) Å^3	V = 244.58(8) Å^3
Z	4	4	4
Space group	*Pnma* (no. 62)	*Cmcm* (no. 63)	*Cmcm* (no. 63)

579 [a]Synthesized at 27 GPa and 2500 °C

580 [b]Synthesized at 45 GPa and 1727 °C

Table 3. Average interatomic distances and coordination numbers of cations in new low-density $CaFe_2O_4$-related and $CaTi_2O_4$-type $MgAl_2O_4$.

New low density $CaFe_2O_4$-related					
^{aV}Mg−O	2.031 Å	^{aVI}Al1−O	1.952 Å	^{aV}Al2−O	1.860 Å
n_c	4.72	n_c	5.98	$^{aV}n_c$	4.23
				$^{aIV}n_c$	3.98
$CaTi_2O_4$-type synthesized at 27 GPa and 2500 °C					
^{aVI}Mg−O	2.144 Å	^{aVI}Al−O	1.928 Å		
^{aVIII}Mg−O	2.248 Å	n_c	5.84		
$^{aVI}n_c$	5.49				
$^{aVIII}n_c$	5.89				
$CaTi_2O_4$-type synthesized at 45 GPa and 1727 °C					
^{aVI}Mg−O	2.152 Å	^{aVI}Al−O	1.936 Å		
^{aVIII}Mg−O	2.259 Å	n_c	5.84		
$^{aVI}n_c$	5.74				
$^{aVIII}n_c$	5.98				

Abbreviations: n_c: effective coordination number.

[a]IV, V, VI, and VIII indicate the values calculated using the four, five, six, and eight nearest neighbor oxygen-cation bonds, respectively.

586 **Table 4.** Molar volumes and densities of phases with $MgAl_2O_4$ composition

Phase	V_m (cm^3/mol)	ρ (g/cm^3)	Reference
New low-density $CaFe_2O_4$-related	40.66(1)	3.499(1)	This study
Sp	39.760(3)	3.578(1)	[1]
MgO Pc + Al_2O_3 Cor	36.853(5)	3.860(1)	[2], [3]
1/2(mLd-type $Mg_2Al_2O_5$ + Al_2O_3 Cor)	36.809(3)	3.865(1)	[4]
CF-type	36.136(3)	3.937(1)	[5]
	36.17(2)	3.933(1)	This study
CT-type	36.368(8)	3.912(1)	[a]This study
	36.82(1)	3.864(1)	[b]This study
	36.23(2)	3.927(3)	[6]

587 Abbreviations: Sp: spinel; Pc: periclase; Cor: corundum; mLd: modified ludwigite; CF: calcium ferrite;
588 CT: calcium titanate.

589 [1] Meducin et al. (2004); [2] Toebbens et al. (2001); [3] Tsirelson et al. (1998); [4] Enomoto et al.
590 (2009); [5] Kojitani et al. (2007); and [6] Ono et al. (2006)

591 [a]Synthesized at 27 GPa and 2500 °C

592 [b]Synthesized at 45 GPa and 1727 °C

593

594

Figure 1

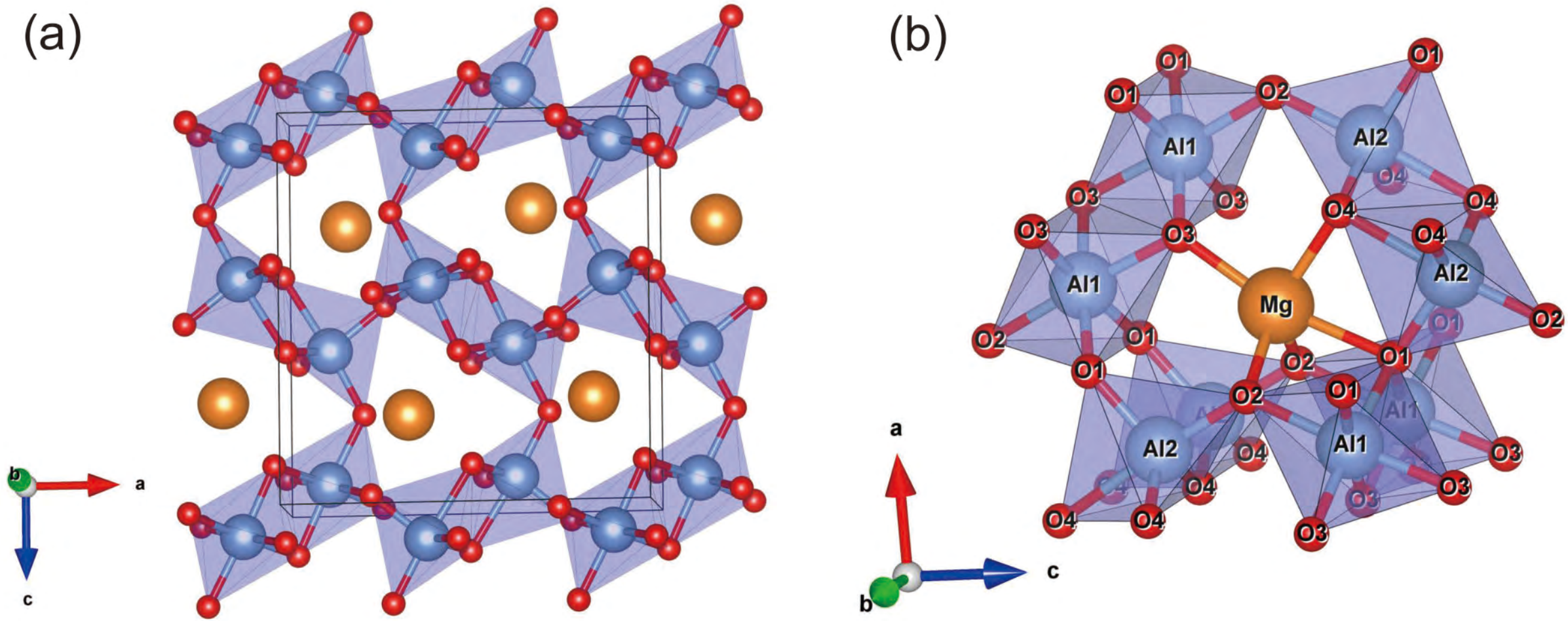

Figure 2

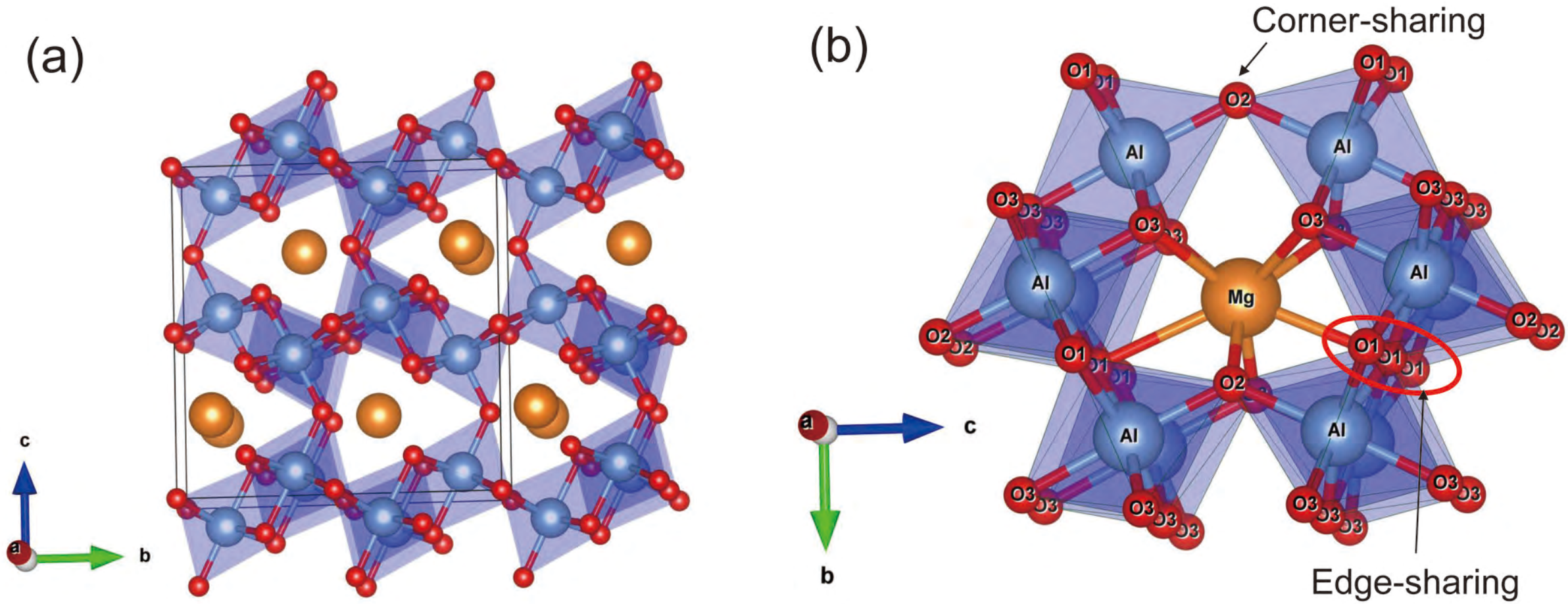

Figure 3

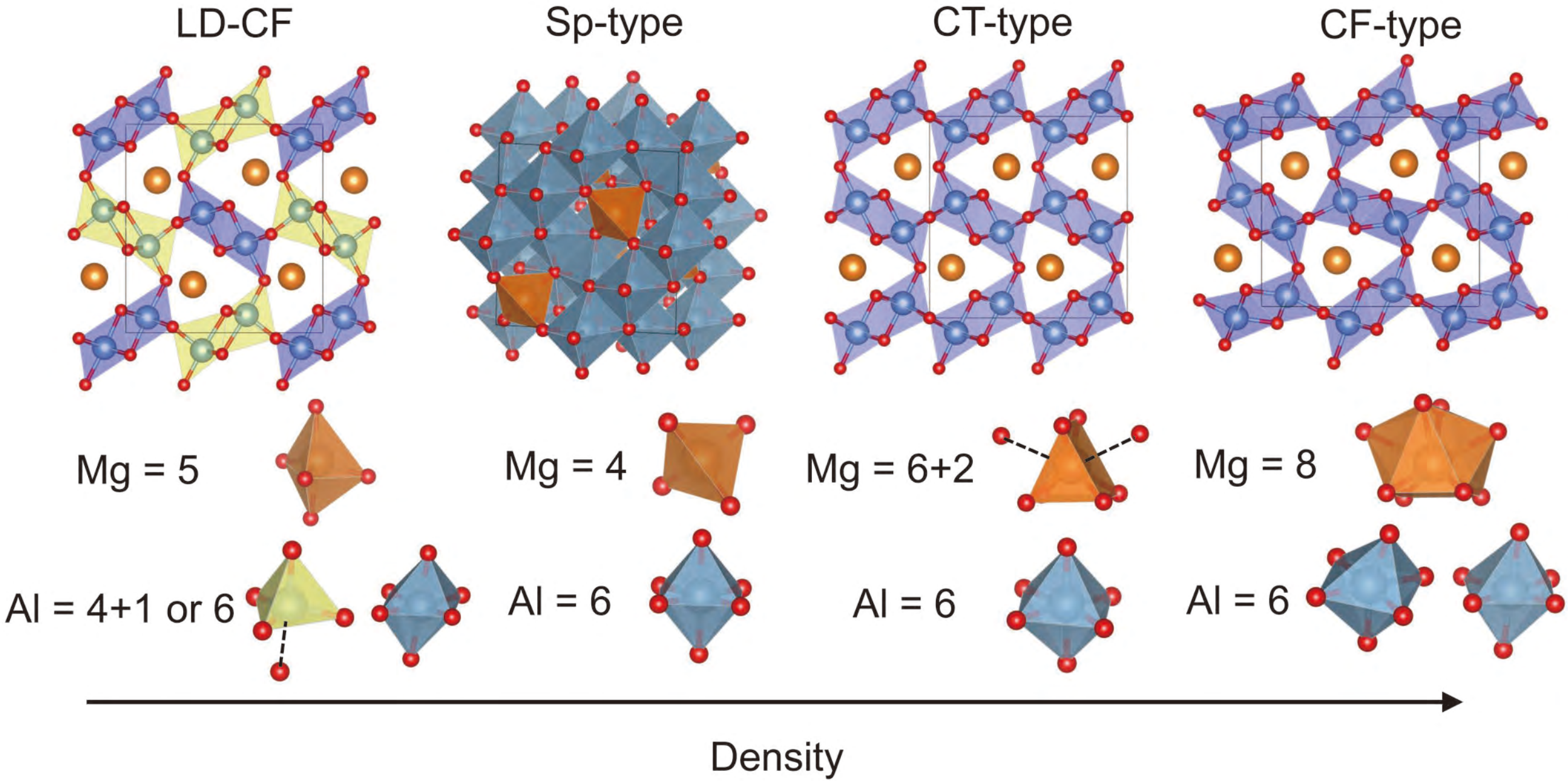
LD-CF
Sp-type
CT-type
CF-type
Mg = 5
Mg = 4
Mg = 6+2
Mg = 8
Al = 4+1 or 6
Al = 6
Al = 6
Al = 6
Density